Journal of Hazardous Materials Advances 17 (2025) 100609

Contents lists available at ScienceDirect

Journal of Hazardous Materials Advances

journal homepage: www.elsevier.com/locate/hazadv

Localization and speciation of rare earth elements in mine tailings from ion-adsorption clay deposits, Southern China: Insights from microfocused X-ray fluorescence spectroscopy

Noémie Janot [a,b,c,*], Hermine Huot [a,d,e], Camille Rivard [f,g], Mathilde Perrin [b], Alexandra Noirault [b], Ye-Tao Tang [d], Françoise Watteau [b], Emmanuelle Montargès-Pelletier [a]

[a] Université de Lorraine, CNRS, LIEC, F-54500 Nancy, 54501, France
[b] Université de Lorraine, INRAE, LSE, F-54500, Nancy, France
[c] INRAE, Bordeaux Sciences Agro, ISPA, F-33140, Villenave d'Ornon, France
[d] School of Environmental Science and Engineering, Sun Yat-sen University, Guangzhou 510275, China
[e] IRD, CNRS, Sorbonne Université, Univ. Paris Est Créteil, INRAE – Institute of Ecology and Environmental Sciences (iEES-Paris), F-75005, Paris, France
[f] SOLEIL synchrotron, L'Orme des Merisiers, F-91190 Saint Aubin, France
[g] INRAE, TRANSFORM, F-44316, Nantes, France

ARTICLE INFO

Keywords:
Regolith-hosted deposits
Soil reclamation
Synchrotron-based spectroscopy
Cerium
Lanthanides

ABSTRACT

Economic exploitation of Ion-Adsorption Rare Earth Elements (REEs) Deposits, a type of ore specific to southern China, has been traditionally performed by heap leaching, creating large amounts of tailings. To design sustainable reclamation techniques for these sites, an understanding of the speciation of residual REEs in the tailings is needed. The aim of the present study was to identify the REE-bearing phases in reclaimed and non-reclaimed tailings from a demonstration site in Dingnan, Jiangxi province, China, in undisturbed soil thin sections using synchrotron-based microfocused X-ray spectroscopy. Bulk and microscale results showed that REEs were concentrated in the fine fraction (<50 µm), mainly dispersed within a heterogeneous micrometric matrix. Using micro-spectroscopy, micro-hotspots of Ce(IV) were evidenced, assigned to CeO_2 microparticles, unaffected by the leaching treatment and dispersed in the tailings. Analyses performed on reclaimed tailing samples (amended with organic substances and planted) showed the high affinity of REEs for organic phases, even at very low concentration, suggesting a significant positive impact of phytoremediation onto REE fate in this post-mining context.

Introduction

Rare Earth Elements (REEs) are a group of elements of close chemical behaviour and specific electronic and magnetic properties that are crucial for manufacturing modern electronics. Their numerous industrial applications, together with their increasing need for various high-technology products as well as for the development of sustainable energy, make them classified as critical materials (Jowitt et al., 2017, and references therein). Currently, China covers about 80 % of the world REEs production, in particular through the mining of Ion-Adsorption Clay Deposits (IAD), also referred to as regolith-hosted clay or weathered-crust elution deposits, which supply about 20 % of the world production and >95 % of the production of heavy REEs (Riesgo García et al., 2017; Sanematsu and Watanabe, 2016). These REE-enriched deposits are generated by the weathering of granitic bedrocks under subtropical climate (Li et al., 217). They are currently mined in China only, but similar occurrences have been found across a larger subtropical area, including Southeast Asia (Sanematsu et al., 2013, 2009) and Madagascar (Berger et al., 2014; Borst et al., 2020; Janots et al., 2015; Ram et al., 2019). In the past few years, characteristics of IADs including mineralogy and associated REE chemical status have been reported in several publications (Borst et al., 2020; Huang et al., 2021; Li and Zhou, 2020; Mukai et al., 2020; Ou et al., 2022; Ram et al., 2019; Sanematsu and Watanabe, 2016; Wu et al., 2023). During the weathering and the dissolution of parent minerals, REEs are released and adsorbed onto clay minerals downwards through surface complexation including ion exchange (Borst et al., 2020; Wu et al., 2023). Chemical extractions evidenced four carrying phases for REEs in IADs: water soluble,

* Corresponding author at: INRAE, Bordeaux Sciences Agro, ISPA – UMR 1391, 71, Avenue Edouard Bourlaux, 33882 Villenave d'Ornon cedex, France.
E-mail address: noemie.janot@inrae.fr (N. Janot).

https://doi.org/10.1016/j.hazadv.2025.100609
Received 5 September 2024; Received in revised form 7 January 2025; Accepted 15 January 2025
Available online 22 January 2025

ion-exchangeable, colloidal sediment (oxides-bound) and mineral phases (Chi et al., 2005; Voßenkaul et al., 2015). The ion-exchangeable phase is the major pool, with >50 % (and up to 90 %) of REEs present as hydrated trivalent cations weakly adsorbed onto clay minerals (clay mineralogy is dominated by 7 Å type, kaolinite or halloysite) or onto other oxides (Fe and Mn oxides) (Li and Zhou, 2020; Pan et al., 2023; Wang et al., 2018). Recent analysis carried out on two IAD-like ores using synchrotron X-ray absorption spectroscopy (XAS) has shown that REEs were indeed adsorbed as easily-leachable outer-sphere hydrated complexes, dominantly onto kaolinite (Borst et al., 2020).

REEs are trivalent elements, except for cerium Ce and europium Eu that have variable valences (Ce(IV) and Ce(III); Eu(II) and Eu(III)) in the environment, inducing positive or negative anomalies in the REE distribution patterns (*i.e.*, enrichment or depletion in Ce and Eu compared to REEs of close atomic number). These anomalies can be used as tracers of soil and redox processes (Laveuf and Cornu, 2009). In IAD material, REE patterns usually display negative Ce anomalies, due to the presence of oxidized Ce(IV) as cerianite (CeO_2) and/or to the scavenging of Ce by Fe/Mn oxides (Li et al., 2020; Ram et al., 2019). Microscopic analyses made on an IAD ore from Madagascar using complementary quantitative evaluation of minerals by scanning electron microscopy (QEMSCAN) and Synchrotron X-ray micro-fluorescence mapping (micro-XRF) demonstrated a high mineralogical heterogeneity. XAS data showed for this ore the co-existence of trivalent and tetravalent Ce, Ce(IV) being associated with Mn-Fe-rich areas (Ram et al., 2019).

The REE grades of ores from exploited IADs range from 140 to 6500 mg kg^{-1}, with an average at 800 mg kg^{-1} (Sanematsu and Watanabe, 2016). These REE deposits are relatively low concentrated compared to igneous ones such as hydrothermal ores (ex. Bayan Obo, China) or carbonatites (ex. Mt. Pass, USA) in which the REE grades can exceed 5 % (50,000 mg kg^{-1}, Kanazawa and Kamitani, 2006). However, the traditional mining of IADs by heap leaching, a low-cost process, makes them economically viable (Nie et al., 2020). After vegetation removal and excavation of the topsoil, the REE-enriched soil clayey layer is leached with a mildly acidic solution of ammonium sulfate. The REEs weakly adsorbed onto clay minerals are desorbed through ion exchange by exceeding cations (NH_4^+) (Moldoveanu and Papangelakis, 2013). This relatively easy recovery process has been performed at a large scale for several decades, producing millions of tons of tailings and leading to severe environmental damages on surrounding environments in South China (Yang et al., 2013). During the mining process, leaching solutions enriched in ammonium, sulfate and various metals can be discharged into surrounding streams and cause pollution of water, sediments and irrigated agricultural soils (Liu et al., 2019). Tailings are subject to leaching and erosion in the subtropical climate as it is difficult for plants to grow on these sandy materials which are poor in organic matter and nutrients. Reclamation of these tailings is therefore an important issue in the mined areas. Different strategies can be considered: (i) using natural processes of revegetation (Guo et al., 2022), (ii) establishing a vegetation cover of grasses and legumes (Zhou et al., 2015), (iii) cultivating plants of economic interest, such as fiber or energy crops (Liu et al., 2022; Segovia et al., 2021) or (iv) recovering residual REEs in the tailings by cultivating hyperaccumulating plants and extracting REEs from the plants (Liu et al., 2018; W.-S. Liu et al., 2020; Jally et al., 2021) or directly extracting REEs from the tailings by hydrometallurgy and pyrometallurgy (Zhou et al., 2021; F. 2023).

Whatever strategy is chosen, it is essential to understand the speciation of REEs in the tailings, *i.e.*, the organic or mineral phases with which they are associated, which controls their bioavailability and the risks of dispersion in the environment (Laveuf and Cornu, 2009; Galhardi et al., 2020). For example, it has been shown that REEs association with dissolved organic matter decrease their bioaccumulation in various aquatic organisms (Lachaux et al., 2022a, 2022b, 2023). Due to the non-selectivity of the leaching solution during mining process, tailings can still contain a significant fraction (up to 58 %) of initial REE amount, with concentration up to 1148 mg kg^{-1} reported (Liu et al., 2019). Chemical extractions performed on IAD tailings samples showed a loss of the exchangeable pool after mining, but studies on different IAD sites showed contrasted results on the speciation of REEs in the tailings, the major part being either the residual pool, *i.e.*, incorporated into the crystal structures of primary and secondary minerals, or still as ion-exchangeable species (Ou et al., 2022; Zhou et al., 2021). Cerium, though, has been found to be essentially coprecipitated with Fe/Mn oxides in the colloidal phase (Zhou et al., 2021). Sequential extractions can induce redistribution of elements during experimental procedure, leading to misinterpretation of experimental results (Gómez-Ariza et al., 1999). To decipher metal speciation in intact material, it is then important to use complementary techniques of direct investigation.

The main objective of this work was to investigate the REE localization and chemical speciation in non-reclaimed and reclaimed IAD tailings, using direct investigation techniques to detect REEs *in situ* in soil samples. Using synchrotron micro-XRF and spatially resolved X-ray absorption spectroscopy (micro-XAS), we investigated the distribution of REEs at the micron scale in thin sections made from the mine tailings. The samples were selected from a demonstration site in China testing different reclamation practices on abandoned tailings resulting from IAD mining. These results provide insight on the impact of reclamation practices (addition of organic amendment, planting) on REE speciation and localization in IAD mine tailings, in order to make assessments on the future management of such REE-contaminated areas.

Material and methods

Study area and sampling

Site description

The studied site was located in an area impacted by IAD mining in the Dingnan county of Ganzhou city, Jiangxi province, China (Figure S1–1 of supplementary information). The weathered crusts were derived from a monzonitic granite from the early Yanshanian period (Jurassic). The parent granitic rocks of the Dingnan area are fine- to coarse-grained biotite granite containing REE-bearing accessory minerals including zircon, apatite and fluorocarbonates (synchisite) (Ishihara et al., 2008; Li et al., 2017). The weathered crusts from these granites were mainly composed of quartz, potassic feldspars and kaolinite while biotite and plagioclase were mostly weathered. They host IAD enriched in light REEs (LREEs) with positive Ce anomaly (Li et al., 2017; Murakami and Ishihara, 2008). The subtropical monsoon humid climate of the region was characterized by an average annual temperature of 18.8 °C and average annual precipitations of 1609 mm (Dingnan County People's Government Network).

On this site, IADs have been mined for REEs until 2008. The tailings resulting from heap leaching technique cover an area of 0.5 km^2 and were landscaped in 2011. Since 2015, this site has been used as a demonstration site for the revegetation of ion-adsorption REE mine tailings. In this study, two zones of this demonstration site were sampled to investigate the distribution of REEs in the tailings: (i) small-scale experimental plots set up to test different strategies of phytoremediation, including unreclaimed tailings (*control* sample) and tailings amended and planted with a native grass (*miscanthus* sample) and (ii) a field plot implemented to test the production of fiber plants on the tailings (*ramie* sample) (Fig S1–1).

Experimental plots (control and miscanthus samples). Experimental plots (13 treatments x 5 plots, 2 x 2 m each) were set up in July 2016 to monitor several strategies of phytoremediation (Y. Liu et al., 2020). The five plots of unreclaimed bare tailings used as controls were sampled in November 2016. Plots amended with a mixture of pig manure and sawdust and planted with a native grass, *Miscanthus sinensis*, were also studied. The organic amendment was added at a rate of 2.6 kg m^{-2} and mixed manually with the first 10 cm of the tailings. Soil samplings were

done on each of the five plots in November 2017, 16 months after planting. A 30 cm deep pit was dug for one of the five plots in order to describe soil profiles (Fig S1–2).

Field plot with fiber plants (ramie samples). Fiber plants were grown on the tailings in a field plot of 1700 m^2 at the demonstration site (zone A; Liu et al., 2022). In July 2015, a mixture of pig manure and sawdust was added as amendment at a rate of 5–6 kg m^{-2} and mixed with the first 10 to 12 cm of the tailings by tillage. Then the plot was sown with an annual fiber plant. In June 2016, the plants were removed, the soil was amended with the same mixture at a rate of 1.5–3 kg m^{-2}, tilled and planted with a perennial fiber plant ramie (*Boehmeria nivea* L. Gaudich). In November 2017, five pits were dug (60 cm in depth) across the field plot to study root and soil development in the tailings (Fig S1–2). Soil profiles were described and delimited into different layers based on their visual aspect and differences of color, structure, compactness and relative content in roots and stones (> 2 mm).

Sampling

For each plot, a composite bulk soil sample (100 to 1000 g) was collected on the surface (0–10 cm). To study the microstructure, blocks of undisturbed material were collected on the surface of the tailings (0–9 cm) and at different depths along the profiles using Kubiena boxes (90 x 60 x 50 mm). The metallic boxes were inserted slowly into the soil and excavated using a knife. Then they were wrapped and placed in a container to minimize dehydration and disturbances during the transport to the laboratory.

Bulk soil sample preparation and analyses

The bulk surface soil samples (n = 5 for control, Miscanthus and ramie treatments) were air-dried and sieved at 2 mm before analysis. An aliquot was subsequently ground (< 150 μm) for chemical and mineralogical analyses.

Elemental composition

Total elemental concentrations were measured on ground soil samples at ALS Chemex Co. Ltd (Guangzhou, China). After lithium borate alkaline fusion, element concentrations were analyzed by X-ray fluorescence spectrometer (PANalytical PW2424, Netherlands) for major elements *(i.e.,* Si, Al, K, Fe, P*)* and ICP-MS (Agilent VISTA, USA) for REEs. For REEs, the detection limits ranged from 0.01 to 0.5 mg kg^{-1}. Total carbon and nitrogen concentrations were determined by dry combustion using an elementar analyzer (Vario EL Cube, Elementar, Germany) at the Sun Yat-sen University analytical center (Guangzhou, China).

Chemical extractions and pH

The soil pH was measured from the suspension of air-dried < 2 mm soil in deionized water at a ratio 1:2.5 (w/v) using a pH-meter (PHSJ-3F INESA, China). The cationic exchange capacity (CEC) and exchangeable cations were analyzed using the cobalt hexamine chloride method (NF ISO 23,470). The CEC was determined by spectrophotometry and the concentrations of exchangeable cations (Al^{3+}, Ca^{2+}, K^{+}, Mg^{2+}, Na^{+}) by ICP-OES (Perkin Elmer Optima S300 DV).

Air-dried < 2 mm samples were extracted with a 1 mM $CaCl_2$ solution at a 1:2 (w/w) ratio to estimate the REE concentrations that can be easily released from solid phases to soil solution. After 48 h of contact, samples were centrifuged for 10 mn at 3000 rpm and filtered through a 0.45 μm filter. Filtered samples were acidified at 2 % HNO_3 and $CaCl_2$-extractable REEs concentrations were determined using ICP-MS: Agilent VISTA, USA, at ALS Chemex Co. Ltd, Guangzhou, China for *control* and *ramie* samples, and Perkin Elmer NexION 350D for *miscanthus* samples. The detection limit for REEs in solutions was 0.001 mg l^{-1}.

X-ray diffraction analyses

Mineralogical analyses were carried out on a composite sample of the unreclaimed bare tailings (*control* sample). X-ray diffraction (XRD) analyses were performed at Laboratoire Interdisciplinaire des Ecosystèmes Continentaux (LIEC, Vandœuvre-lès-Nancy, France) on ground bulk samples to determine the major crystalline phases. A D8 Advance Bruker diffractometer with a Co K_{a1} radiation source, operated at 35 kV and 45 mA (λ = 1.7889 Å), was used. XRD patterns were collected on the angular range (2θ) of 3–64°, with a 0.034° step size and a 3 s collecting time.

Data analysis

To study the distribution pattern of REEs, the total concentrations were normalized by the concentrations in the upper continental crust (Taylor and McLennan, 1995). The ratio LREEs/HREEs was calculated as the sum of the normalized concentrations of the light REEs (LREEs, La to Eu) divided by the sum of the normalized concentrations of heavy REEs (HREEs, Gd to Lu). The cerium anomaly (*Ce) was calculated as $2*[Ce]_N/([La]_N+[Pr]_N)$ and the europium anomaly (*Eu) as $2*[Eu]_N/([Sm]_N+[Gd]_N)$ with $[X]_N$ the normalized concentrations.

Data were processed using R software version 3.6.2. (R Core Team, 2022). The data obtained on bulk soils were presented as arithmetic means, standard deviation and median calculated on five replicates for the three sample groups (control, *miscanthus* and *ramie*). Differences in elemental composition and physico-chemical properties between these groups were assessed using Kruskal-Wallis test followed by a multiple comparison test at a significant level of 0.05 with *pgirmess* R-package (Giraudoux, 2023).

Particle size fractionation and analyses

Size fractionation was performed on the composite control sample in triplicate. 10 g of sample (size fraction < 2 mm) were gently dispersed in 200 ml of distilled water and agitated for 1 h in a rotative agitator at 15 tr min^{-1}. Size fractions were obtained by wet sieving at 250 and 50 μm and were subsequently dried, ground and analyzed for organic C (Unicube equipment, Elementar) and major elements using ICP-OES (iCAP Pro Duo X, Thermo) at the Laboratoire Sols et Environnement (LSE, Vandœuvre-lès-Nancy, France), and for REEs using ICP-MS at the Service d'Analyse des Roches et Minéraux (SARM, CRPG, Vandœuvre-lès-Nancy, France). Supplementary XRD analyses were performed on the fine fraction (< 50 μm).

An aliquot of this fine fraction (< 50 μm) was suspended in ethanol and ultrasonicated to enhance particle dispersion. One drop of the suspension was deposited on a Cu grid coated with a carbon thin layer for subsequent Transmission Electron Microscopy (TEM) analyses. TEM analyses were carried out using a CM200 Philips TEM with 200 kV accelerating voltage at Institut Jean Lamour (IJL, Nancy, France). The electron microscope was coupled with an EDAX EDXS spectrometer.

Thin section preparation and analyses

Thin sections preparation

Thin sections were prepared at the LSE from the blocks of undisturbed samples collected in the tailings. Samples collected in Kubiena boxes were dried with acetone, embedded in polyester resin and polymerized at 35 °C. Each consolidated block was split in two and one part was glued on glass slide. Then the glued block was refined to obtain a 30 μm thick section (50 x 80 mm).

Microscopic analyses

Thin sections of the different samples were first observed using a stereomicroscope (Leica MZ FLIII, Leica Microsystems AG, Heerbrugg, Switzerland). Descriptions of the mineral and organic components and microstructural features were made following the guidelines of Bullock et al. (1985) and Stoops et al. (2010). Specific mineral and organic

phases were further analyzed on one thin section of *ramie* sample with a scanning electron microscope TESCAN VEGA 3 LM coupled with EDS detector Bruker XFlash6 30 mm^2 and cathodoluminescence system Gatan ChromaCL2UV at the Service Commun de Microscopie Électronique et de Microanalyse X (SCMEM, UL-CNRS, Vandœuvre-lès-Nancy, France). The analyses were performed on the thin section without carbon coating at low vacuum (20 Pa) and at 15 keV.

Synchrotron X-ray fluorescence at SOLEIL

Data acquisition. Micro-XRF analyses on three thin sections, one made in the surface of tailings amended and planted with miscanthus (*miscanthus* sample) and two made in the surface of tailings amended and planted with ramie (*ramie* sample) (one horizontal and one vertical; Fig. S4–2, 3 and 4). Analyses were carried out on the LUCIA beamline at SOLEIL Synchrotron (Gif sur Yvette, France), using a double crystal Si(111) monochromator. Micro-XRF elemental maps were collected at 7200 eV, above Fe and Mn K-edges and La, Ce and Nd L_3-edges. The X-ray beam was focused to 3.0 × 3.0 (v × h) μm^2 by means of a Kirkpatrick-Baez mirror arrangement. The XRF signal was collected using a 60 mm^2 silicon drift diode Bruker detector in continuous FlyScan mode acquisition. The pixel size was 10 × 10 μm^2 for the low spatial resolution maps and 3 × 3 μm^2 for the high spatial resolution ones with an integration time of 100 ms and 200 ms per pixel, respectively.

Data processing (fluorescence signal deconvolution). The energy resolution of the detector allows us to identify the fluorescence lines of the elements of interest, thereby directly displaying several elemental maps at the beamline using energy region of interest (eROI) around the elements. However, as others have reported it before, REEs (Ce, La mainly) elemental maps showed strong interferences with other trace elements (Ti, Ba) (Stuckman et al., 2018). Indeed, several overlaps are possible in such complex media: the main La Lα line signal is at 4647 eV, close to the Ti Kα line at 4512 eV. Ce Lα line signal is at 4839 eV and can be interfered by Ba Lβ line at 4828 eV. To optimize the discrimination of the various XRF line contributions, the XRF signal of each element was extracted by batch fitting the XRF spectrum in each pixel of the map using the PyMCA software (Solé et al., 2007). This process allowed us to display elemental maps for Al, Ca, Cl, Cr, Fe, K, Mg, Mn, Na, P, S, Si, Ti, V (based on K fluorescence lines) and Ba, La, Ce, Nd (based on L fluorescence lines). The count number for the XRF signal was normalized by the count number of the incoming beam signal and corrected by the XRF detector deadtime. Three color RGB (Red-Green-Blue) maps were generated to display spatial correlation using the Fiji software (Schindelin et al., 2012). Examples of differences between eROI-based and PyMCA-fitted maps can be found in Appendix S2 of supplementary information.

REE L-edge X-ray absorption near edge structure (XANES). Micro-XANES spectra were collected at the L_3-edges of La, Ce and Nd to check the presence of these REEs at selected points of interest (POIs) with low contents in REEs. Moreover, the acquisition of XANES spectra was also a means of tracking the oxidation state of Ce, which is known to display variable oxidation state, Ce(III) or Ce(IV). XANES spectra were recorded on short range of energy at L_3-edge of La (5420 to 5620 eV), Ce (5650 to 5870 eV) and Nd (6100 to 6400 eV), with 0.2 eV energy step and counting time of 200 ms per point, using continuous FlyScan mode. The acquisition of fast successive spectra did not reveal any modification of spectral features, indicating that oxidation state was not impacted by beam damage, in particular for Ce.

Fe K-edge XANES. As the thin sections display several features indicating the presence of Fe-(hydr)oxides, we aimed at revealing the nature of Fe-bearing phases in the tailing material. To do so, since XRD was inadequate due to the low Fe content and the low-crystallinity of Fe-phases, we performed XAS analysis at the Fe K-edge. Fe K-edge micro-XANES were acquired on multiple POIs, on the energy range 7050–7250 eV, with 0.2 eV energy step and counting time of 200 ms per point using continuous FlyScan mode. Fe K-edge spectra were compared to Fe reference spectra collected on LUCIA beamline with the same energy resolution: goethite, ferrihydrite, lepidocrocite and clay minerals (illite, montmorillonite, bentonite). Linear combination fitting (LCF) was performed using Athena software (Ravel and Newville, 2005). For each spectrum, the E_0 edge energy was chosen as the maximum of the first derivative of the XANES spectrum. Tailing samples and reference spectra were all normalized in the same energy domain [−20, +100] around E_0. LCF was performed on a restrained energy domain [−20; +80], with a maximum number of components set to 3 and the sum of contributions forced to be equal to 1. The fitting solution was judged by the lowest R_x factor and the number of components was increased only if it resulted in a consistent decrease in R_x (higher than 10 %). The fitting solution was selected not only from the lowest residual component but also from visual appreciation (Ravel and Newville, 2005).

Results

Characteristics of the tailings

The tailings were composed mainly of Si, Al, Fe and K and showed very low concentrations of C and nutrients (Table 1). Even after ore extraction through leaching, the tailings still showed relatively high residual REE concentrations with high spatial variability across the site; the sum of REE concentrations varying from 254 to 1627 mg kg^{-1}. Control tailings were acidic (pH < 5) with a low CEC saturated by Al^{3+}. The reclamation practices induced significant changes in the composition and some chemical properties of the tailings (Table 1). Planting and

Table 1
Elemental composition and some chemical parameters of the bulk soil samples of unreclaimed tailings (control) and tailings amended and planted with miscanthus or ramie
The results are presented as mean ± standard deviation (median) calculated on 5 samples per treatment. Different letters indicate significant differences between the treatments ($p < 0.05$) using Kruskal-Wallis test followed by multiple comparison test. ΣREEs: sum of the concentrations of the 14 REEs (La to Lu); CEC: cationic exchange capacity; S/T: nonacid saturation (sum of exchangeable concentrations of Ca^{2+}, Mg^{2+}, K^+ and Na^+ divided by the CEC); Al/T: aluminium saturation (exchangeable concentration of Al^{3+} divided by the CEC).

Samples		Control	Miscanthus	Ramie
Total elemental composition				
Si	%	33.5 ± 0.4 (33.4) [a]	32.4 ± 0.4 (32.2) [ab]	30.8 ± 1.4 (31.0) [b]
Al	%	8.3 ± 0.2 (8.2) [a]	8.6 ± 0.3 (8.6) [a]	8.7 ± 0.8 (8.4) [a]
K	%	4.5 ± 0.2 (4.4) [a]	4.3 ± 0.1 (4.3) [ab]	3.9 ± 0.1 (4.0) [b]
Fe	%	2.1 ± 0.4 (2.2) [b]	2.6 ± 0.4 (2.6) [ab]	2.8 ± 0.1 (2.8) [a]
C	%	0.09 ± 0.02 (0.09) [b]	0.46 ± 0.06 (0.48) [ab]	1.8 ± 0.5 (1.8) [a]
N	g kg^{-1}	0.08 ± 0.05 (0.10) [b]	0.36 ± 0.03 (0.36) [ab]	1.6 ± 0.4 (1.5) [a]
P	g kg^{-1}	0.04 ± 0.00 (0.04) [b]	0.11 ± 0.02 (0.09) [ab]	0.74 ± 0.21 (0.66) [a]
ΣREEs	mg kg^{-1}	355 ± 65 (384) [a]	425 ± 81 (422) [a]	865 ± 739 (381) [a]
pH *and cationic exchange capacity*				
pHwater	-	4.6 ± 0.1 (4.6) [b]	4.5 ± 0.1 (4.5) [b]	5.3 ± 0.3 (5.3) [a]
CEC	$cmol^+kg^{-1}$	2.7 ± 0.5 (2.9) [b]	3.0 ± 0.3 (2.9) [b]	5.9 ± 1.3 (5.6) [a]
S/T	% of the CEC	3.4 ± 0.2 (3.4) [b]	28 ± 3 (28) [ab]	113 ± 7 (112) [a]
Al/T	% of the CEC	77 ± 5 (78) [a]	46 ± 13 (53) [ab]	2.3 ± 2.6 (1.0) [b]

amendment both increased the total concentrations of carbon and nutrients (N, P), pH, CEC, non-acid saturation and decreased the Al saturation of the adsorbent complex. Furthermore, ramie planting may have induced a K depletion in the tailings.

In accordance with chemical composition, XRD patterns obtained on bulk powders of the control sample were predominated by crystalline silicates, quartz and potassic feldspars (Appendix S3 – Figure S3–1). XRD patterns on clay fractions demonstrated the presence of various phyllosilicates: chlorite-type (with a line at 14 Å), mica-type (10 Å) and kaolinite-type (7 Å). Complementary TEM observations on the fine fraction evidenced halloysite as the predominant 7 Å phase (Figure S3–2). The total content of Fe was relatively low (<5 %), andFe-bearing minerals could not be detected through XRD. However, TEM observations evidenced the presence of submicrometric amorphous Fe (hydr)oxide phases.

Bulk distribution and extractability of REEs

The concentrations of REEs varied greatly across the field plot planted with ramie, reaching very high concentrations in some sampling points. The most abundant REEs were La, Ce, Nd as well as Y (*Table 2*). There was no significant difference in the distribution of the total concentrations of REEs between the non-reclaimed tailings (control) and those amended and planted with miscanthus or ramie. All the tailing samples showed an enrichment in heavy REEs compared to the light REEs (LREEs/HREEs < 1). The Ce anomaly was positive (*Ce > 1) in the control samples and, to a lesser extent, in the tailings planted with miscanthus. However, it was negative (*Ce < 1) in some samples of tailings planted with ramie. All the samples displayed a negative Eu anomaly (*Eu < 1).

REEs were not easily extracted by millimolar $CaCl_2$ solution, used as a proxy of soil solution. In the unreclaimed tailings (control), the extractible proportion represented 0.7 to 1.7 % of the total concentrations, except for Ce (0.1–0.2 % of the total) (Fig. 1). The extractability of REEs was lower in the reclaimed tailings, especially for those planted with ramie. In all the samples, Ce showed a specific behavior, being less extractible than the other REEs.

Compared with their concentrations in the bulk samples (< 2 mm), REEs were enriched in the smallest size fraction (< 50 μm), together with organic C, Al and Fe (Fig. 2). Only Ce distribution was different from that of other REEs, being less enriched in both <50 μm and 50–250 μm fractions. Organic C was largely enriched in the smallest size fraction (< 50 μm), and almost absent from the largest fraction (250 μm-2 mm). This latter size fraction was the most important, representing 58.1 ± 1.4 % of the weight of the control sample. The other fractions, 50–250 μm and <50 μm, represented 23.4 ± 1.0 % and 18.5 ± 0.4 % of the whole sample, respectively.

Table 2
Total REEs concentrations and specific distribution ratios obtained in the bulk samples of unreclaimed tailings (control) and tailings amended and planted with miscanthus or ramie, determined by ICP-MS.
The results are presented as mean ± standard deviation (median) calculated on five samples per treatment. The LREEs/HREEs ratio was calculated as the sum of the normalized concentrations of the light REEs (La to Eu) divided by the sum of the normalized concentrations of heavy REEs (Gd to Lu). The cerium anomaly (*Ce) was calculated as $2*[Ce]_N/([La]_N+[Pr]_N)$ and the europium anomaly (*Eu) as $2*[Eu]_N/([Sm]_N+[Gd]_N)$ with $[X]_N$ the normalized concentrations.

Sample		Control	Miscanthus	Ramie
La	mg kg^{-1}	60 ± 13 (59)	88 ± 32 (74)	258 ± 261 (73)
Ce	mg kg^{-1}	202 ± 29 (200)	200 ± 28 (188)	233 ± 63 (228)
Pr	mg kg^{-1}	11 ± 4 (11)	16 ± 6 (14)	40 ± 40 (13)
Nd	mg kg^{-1}	38 ± 15 (40)	57 ± 18 (51)	126 ± 128 (43)
Sm	mg kg^{-1}	7.9 ± 3.1 (8.5)	11 ± 4 (10)	23 ± 24 (8.3)
Eu	mg kg^{-1}	1.1 ± 0.4 (1.2)	1.5 ± 0.4 (1.4)	3.7 ± 3.5 (1.4)
Gd	mg kg^{-1}	7.7 ± 2.6 (8.0)	12 ± 4.5 (10)	25 ± 25 (8.6)
Tb	mg kg^{-1}	1.4 ± 0.5 (1.3)	2.2 ± 0.9 (2.0)	4.9 ± 5.1 (1.6)
Dy	mg kg^{-1}	9.2 ± 2.7 (9.6)	14 ± 6 (13)	34 ± 36 (11)
Ho	mg kg^{-1}	2.0 ± 0.5 (2.2)	3.0 ± 1.2 (2.8)	7.2 ± 7.5 (2.2)
Er	mg kg^{-1}	6.0 ± 1.6 (6.3)	8.9 ± 3.6 (8.0)	22 ± 23 (7.0)
Tm	mg kg^{-1}	0.9 ± 0.2 (1.0)	1.3 ± 0.5 (1.2)	3.6 ± 3.8 (1.1)
Yb	mg kg^{-1}	5.9 ± 1.3 (6.4)	8.2 ± 2.9 (7.7)	25 ± 28 (7.4)
Lu	mg kg^{-1}	0.9 ± 0.2 (1.0)	1.2 ± 0.4 (1.1)	3.6 ± 4.0 (1.1)
Y	mg kg^{-1}	65 ± 13 (66)	102 ± 48 (84)	236 ± 244 (69)
LREEs/HREEs	-	0.56 ± 0.08 (0.58)	0.52 ± 0.09 (0.48)	0.48 ± 0.08 (0.50)
*Ce	-	1.84 ± 0.38 (2.02)	1.31 ± 0.46 (1.30)	1.08 ± 0.74 (1.21)
*Eu	-	0.65 ± 0.08 (0.65)	0.64 ± 0.09 (0.62)	0.77 ± 0.08 (0.76)

Spatial distribution of REEs (thin section analysis)

Micromorphological features of the tailings

Observations of the thin sections at the stereomicroscope gave information about the main mineral and organic phases and their arrangement (Appendix S4). Complementary SEM-EDS analyses helped to specify the composition of some minerals (Fig. 3).

Main mineral phases distinguished in all the analyzed thin sections were quartz, potassic feldspars and brownish ferro-magnesian phyllosilicates, probably micas or chlorites (Fig. 3a and b). These observations are consistent with the main mineral phases identified in the control sample by XRD and TEM. The size of these phases varied from hundreds of μm to few cm and they can appear isolated, coated or embedded in a fine-grained reddish matrix. Based on SEM-EDS analyses (n = 9), this reddish matrix was composed mainly of Si (18±2 % atomic), Al (14±2 %), Fe (2.9 ± 4.4 %) and K (1.6 ± 1.2 %), indicating a probable mixture of fine-grained orthosilicates, phyllosilicates and Fe oxyhydroxides. In addition, some particles enriched in Ce or in zirconium (Zr) were detected in the reddish matrix (Fig. 3c and d). Quartz minerals displayed often multiple cracks, some of which were filled with reddish fine-

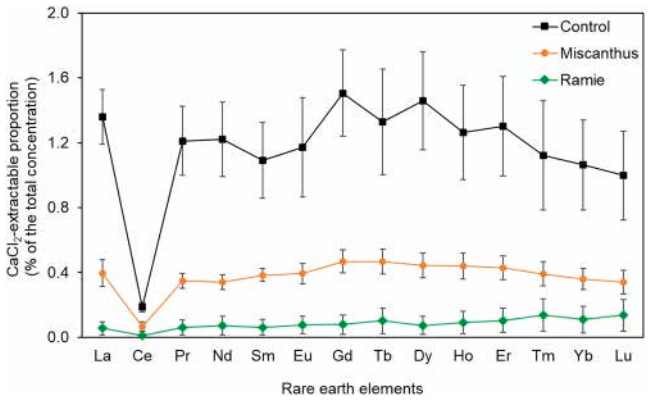

Fig. 1. Distribution patterns of the $CaCl_2$-extractable REE concentrations in unreclaimed tailings (control) and in amended and planted tailings (miscanthus and ramie).
The points represented the average values and the error bars the standard deviation calculated on five samples per treatment.

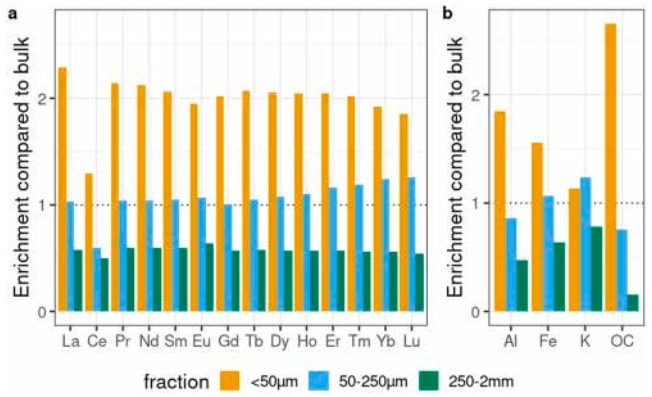

Fig. 2. Enrichment in (a) REEs and (b) major elements and organic carbon (OC) in three size fractions (< 50 µm, 50–250 µm, 250 µm –2 mm) compared to their concentrations in the bulk sample (< 2 mm) of unreclaimed tailings (control sample).

grained matrix. Some ferro-magnesian phyllosilicates also showed marks of weathering and can be surrounded by reddish veins of Fe-enriched particles (Fig. 3e and f). Some yellowish phases enriched in aluminum and containing phosphorus were evidenced (Appendix S4), as well as black particles than can be assigned to Mn (hydr)oxides.

Thin sections from amended and planted tailings (ramie and miscanthus samples), especially those planted with ramie, showed higher proportion of macropores and many roots and organic residues in the voids between minerals (Fig. 3a, c and e, Appendix S4).

REEs in the fine-grained matrix

To investigate the spatial distribution of REEs and identify their bearing phases, elemental maps (obtained from micro-XRF spectra fitting) were recorded on areas of interest, pre-selected from micromorphological observations of the thin sections. From the micromorphological observations (Figs. 3 and S4), a typical mineral assemblage appeared as a recurrent feature of all tailing samples (amended, planted or not). One of its occurrence, crystalline silicate particles (quartz on the right and feldspar on the left) surrounded by a fine-grained matrix, is presented on Fig. 4, from a thin section made in tailings amended and planted with *ramie* (presented in Figure S4–3). The poorly crystalline matrix (which appeared orange-red on optical microscopy pictures, see Figs. 3a & 4a) was constituted of sub-micrometric mineral phases containing Si, Al and Fe (Fig. 4b and corresponding individual elemental maps in Figure S5–1). Fig. 4c shows the presence of a Ce-Mn particle (point of interest POI 1, corresponding fluorescence spectra in Figure S5–2, together with POIs 4, 5 and 7). The fitting of fluorescence spectra allowed us to highlight well-defined micrometric particles of Ce (POIs 2, 3, 5) within the fine-grained matrix. The diffuse pink color of this matrix (POIs 4, 6 to 9) on Fig. 4d, presenting the spatial distribution of the three targeted REEs (La, Ce and Nd) evidenced that it contained both La and Nd. At the scale of the whole map, elemental correlation plots show a very strong correlation between La and Nd ($R^2 = 0.85$), co-localized diffusely in the fine-grained matrix (Fig. 4e). However, at this scale, La was not correlated with Ce ($R^2 = 0.0004$) (Fig. 4f). While La and Nd seemed uniformly dispersed within the fine-grained matrix, Ce was essentially present as hotspots, sometimes co-localized with Mn ($R^2 = 0.63$) (Fig. 4g).

Beside element mapping, micro-XANES spectra at the L_3-edge of La, Ce and Nd, as well as at Fe K-edge were collected on selected POIs (Fig. 4h-k). They showed that Ce was either present as Ce(IV) alone (at POI 1, large Ce-Mn particle), Ce(III) (at POI 4, La/Nd hotspot in the matrix), or as a mixture of Ce(III) and Ce(IV) (at POIs 2, 3 and 5, some of the Ce hotspots in the matrix).

Fe-XANES spectrum was collected on POI 7 to reveal the nature of Fe-bearing phases in this frequently-encountered matrix, and LCF of the spectrum strongly suggested the presence of iron (hydr)oxydes, goethite and ferrihydrite (Fig. 4k). Most occurrences of REEs observed in our samples were found in association with this reddish Fe-rich fine-grained material surrounding silicate grains ($n = 22$ maps on the three thin sections). Other examples of REE-enriched zones in reddish matrix are shown in Appendix S5, on a larger map of the area presented in Fig. 4 (Figure S5–3), or around a quartz grain in the miscanthus sample (Figure S5–4, zone 2).

REEs associated with phosphates

SEM analyses evidenced one occurrence of REEs present along a fracture within yellowish particle enriched in Al and containing P (Fig. 5a and b). Complementary measurements performed by XRF imaging on the same grain showed that REEs (La, Nd, and to a lesser extent Ce) were co-localized with P at the micrometric scale (Fig. 5c-g). Corresponding elemental maps X-ray collected on the grain and the fracture are provided in Figs. S5–5 and S5–6, respectively, and associated fluorescence spectra are shown in Fig. S5–7. The fracture zone displayed strong correlation for La with Nd and Ce (R^2=0.96 and 0.93, respectively) (Fig. 5h-i), evidencing the co-localization of REEs. Micro-XANES measurements performed at several POIs confirmed the presence of La (Fig. 5j), co-localized with Ce, here mainly as trivalent Ce(III) (Fig. 5k).

Despite the large number of maps recorded at LUCIA on three thin sections ($n = 25$ large, low spatial resolution maps), we were not able to detect another occurrence of the association between REEs and phosphates. However, SEM analyses done on other thin sections or on particles from the tailings have confirmed the presence of grains enriched in several REEs (La, Ce, Nd) associated with P (Guo, 2022).

Organic phases in reclaimed tailings

In reclaimed samples, organic material was commonly encountered as plant debris, pieces from the organic amendment or roots. Micro-XRF analyses evidenced their enrichment in REEs ($n = 7$ maps). Fig. 6 shows one of these occurrences in the thin section made in tailings planted with miscanthus, where organic structures bearing S and REEs (La, Ce, Nd, see Fig. 6a-d) were detected. In these structures, REE speciation was extremely similar, as seen by the exact superposition of La, Ce and Nd XANES spectra between POIs 2 and 4 (Fig. 6f-h). Ce was present as trivalent species, as evidenced by Ce L_3-edge XANES measurements (Fig. 6g), but also by the Ce L_2-edge signal in the Nd XANES pre-peak region (Fig. 6h).

As previously observed, Ce in hotspots was Ce(IV) (here co-localized with Ti, see Fig. 6e), whereas Ce in the organic phases, co-localized with other REEs (Fig. 6e), was Ce(III) (Fig. 6g). Corresponding elemental maps can be found in Appendix S5 (Figure S5–8). Similar observations made on thin sections made in tailings amended and planted with ramie are also given there (Figures S5–3 and S5–9). In Figure S5–3, a large plant residue clearly showed an enrichment in La in its external parts. REE presence was not always easy to detect from the fluorescence maps, due to low concentrations and heterogeneous composition of the samples, but was clearly visible in the fluorescence spectra of the organic debris (Figure S5–9).

Discussion

Detection and spatial distribution of REEs in undisturbed tailing samples

The studied samples have a complex historical background: (i) weathering of granitic bedrock in a subtropical climate leading to the formation of REE ion-adsorption deposits, (ii) mining of this ore material by excavation and leaching with ammonium sulfate solution and (iii) abandonment of the remaining tailings, which are subject to leaching and erosion, followed by landscaping and reclamation trials to re-vegetate the site. As a result, they exhibit a high spatial heterogeneity in REE concentrations, both at the macroscopic (bulk samples across the site) and microscopic scale (within a thin section). Throughout the site,

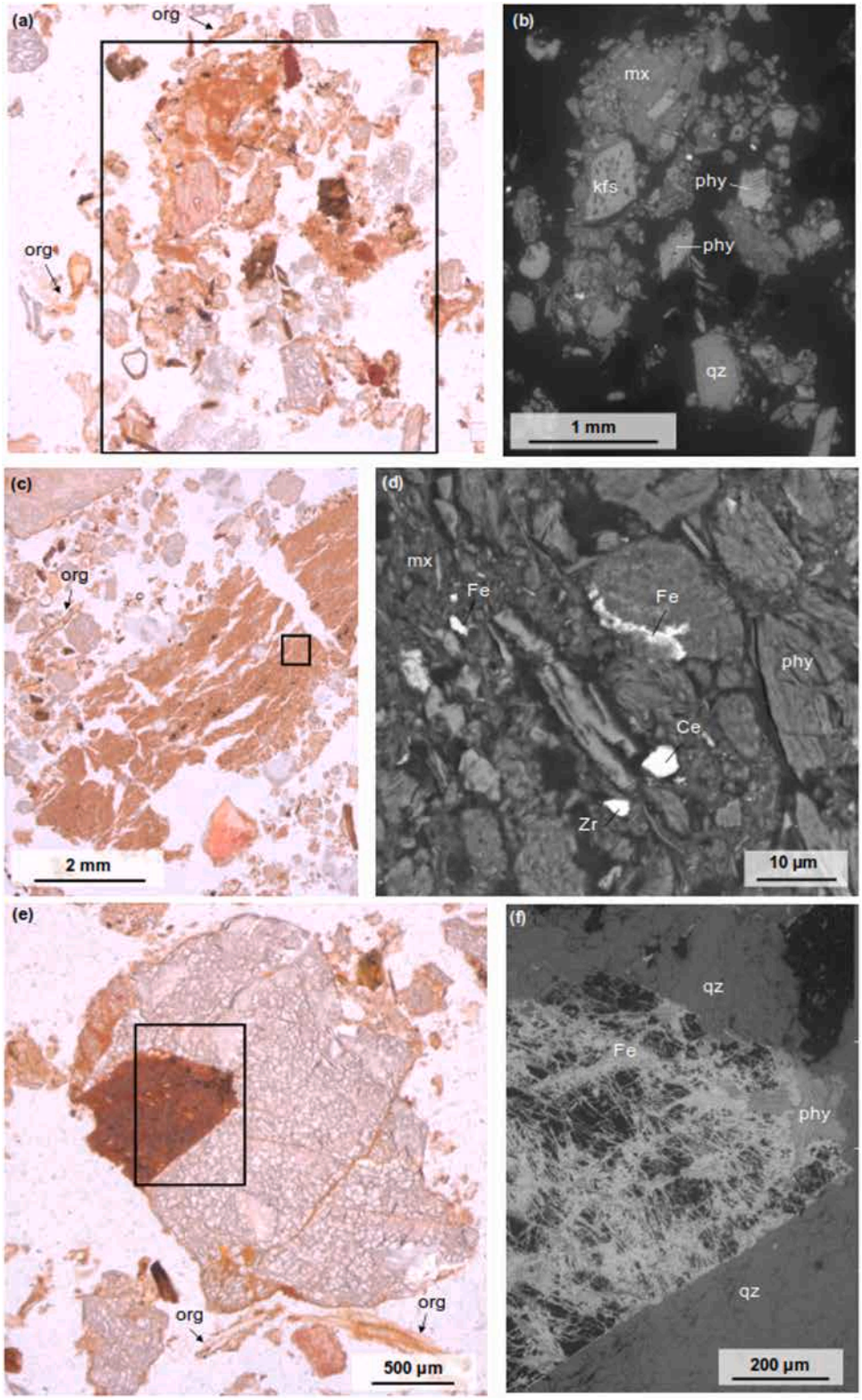

Fig. 3. Optical and backscattered electron images of micromorphological features of the tailings observed on a thin section sampled at the surface of tailings amended and planted with ramie.
(a and b) Assemblage of minerals including quartz (qz), potassic feldspar (kfs) and brownish phyllosilicates (phy) detached or embedded in a reddish fine-grained matrix (mx). Some organic residues or roots (org) were present in voids between minerals.
(c and d) Piece of reddish fine-grained matrix surrounded by detached minerals including quartz and organic residues (org). The matrix was composed of a mixture of micrometric phases including phyllosilicates (phy) and iron oxyhydroxides (Fe) and some particles enriched in cerium (Ce) and zirconium (Zr)
(e and f) Quartz with cracks filled with reddish fine-grained material and a reddish zone of weathering composed of ferro-magnesian phyllosilicates (phy) and veins of Fe-enriched particles (Fe). Roots (org) were developed in the voids between minerals (org).

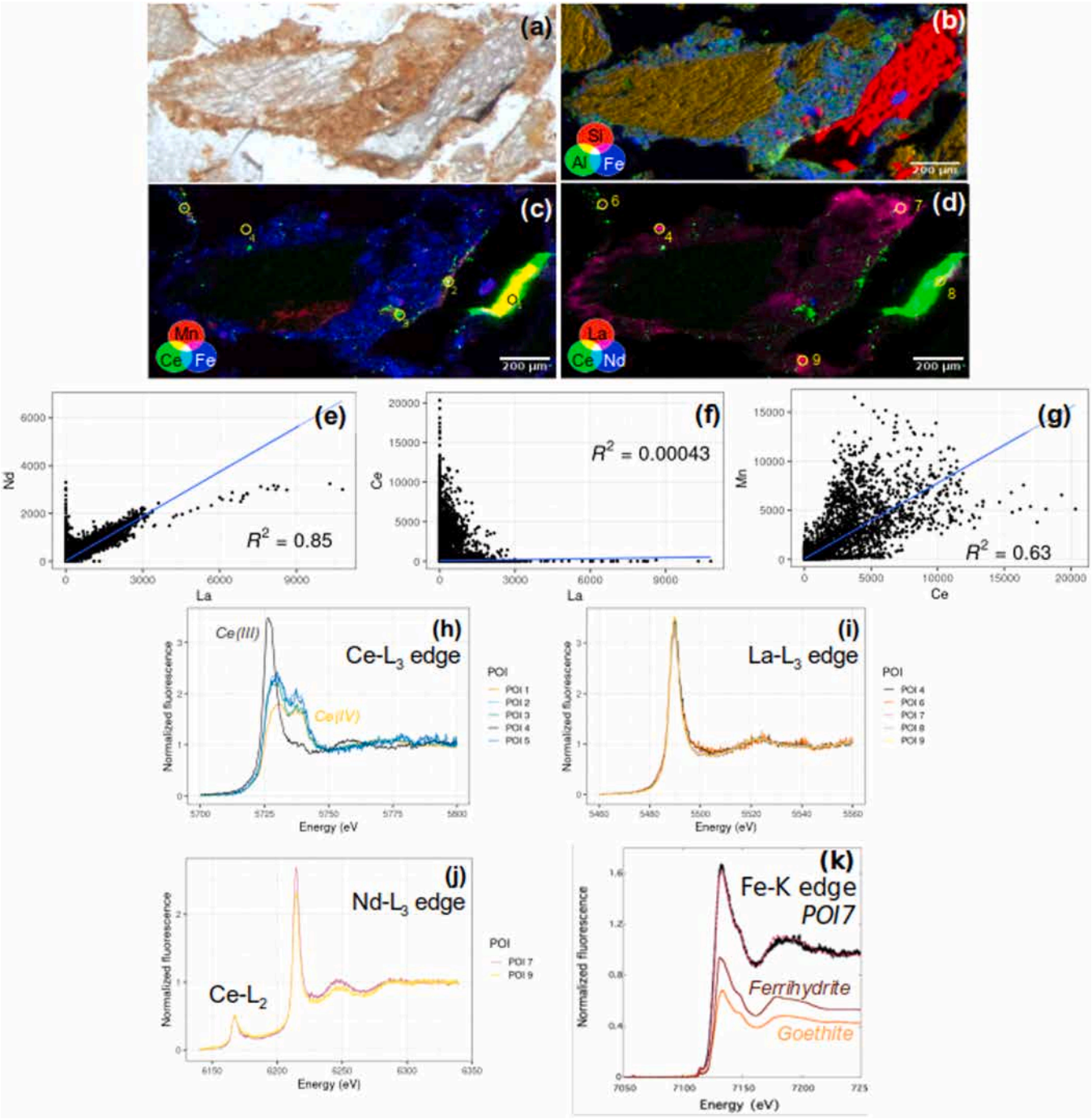

Fig. 4. Optical (a) and tricolor fluorescence (b-d, 3-µm resolution) maps of REEs dispersed in the fine-grained matrix observed in the thin section made in the surface of tailings (0–6 cm) amended and planted with ramie (presented in Fig. S4–3). Correlation plots of Nd-La (e), Ce-La (f) and Mn-Ce (g) established based on signals from all map pixels. Ce (h), La (i), Nd (j), Fe (k, showing LCF using goethite and ferrihydrite) XANES spectra at various locations (POIs) shown in (c-d).

observed residual REE concentrations in the tailings vary from 300 to 2200 mg kg^{-1} (including Y), which largely exceed background soil levels in China (188 mg kg^{-1}) and Jiangxi Province (211 mg kg^{-1}) (Wei et al., 1991), and can reach the concentrations of IAD ores (average at 800 mg kg^{-1}) (Sanematsu and Watanabe, 2016). Therefore, these tailings can be considered as a secondary source of REEs (Zhou et al., 2021). The fractionation patterns show an enrichment in HREEs compared to LREEs, which could result from a preferential leaching of LREEs in the tailings (Liu et al., 2019). We evidenced an enrichment of REEs in fine fraction (<50 µm) of tailing samples, together with Al, Fe and organic C in the tailings, as reported by Zhou et al. (2023). However, neither electron nor synchrotron-based microfluorescence microscopic analysis on isolated fine fraction did allow us to unravel the REE-bearing phases.

To determine REE spatial distribution and speciation, undisturbed samples (thin sections) were prepared, in which the micro-structure, *i.e.*, the arrangement of mineral and organic phases, was kept intact. Main mineral phases include primary granitic minerals (quartz, potassic feldspar, micas), which are more or less weathered, and secondary phases (halloysite, Fe/Mn oxides). Micromorphological observations evidenced the recurrence of a fine-grained matrix, composed of sub-micrometric phyllosilicates (halloysite) and Fe (hydr)oxides, surrounding or covering primary silicate grains from parent granite. Overall,

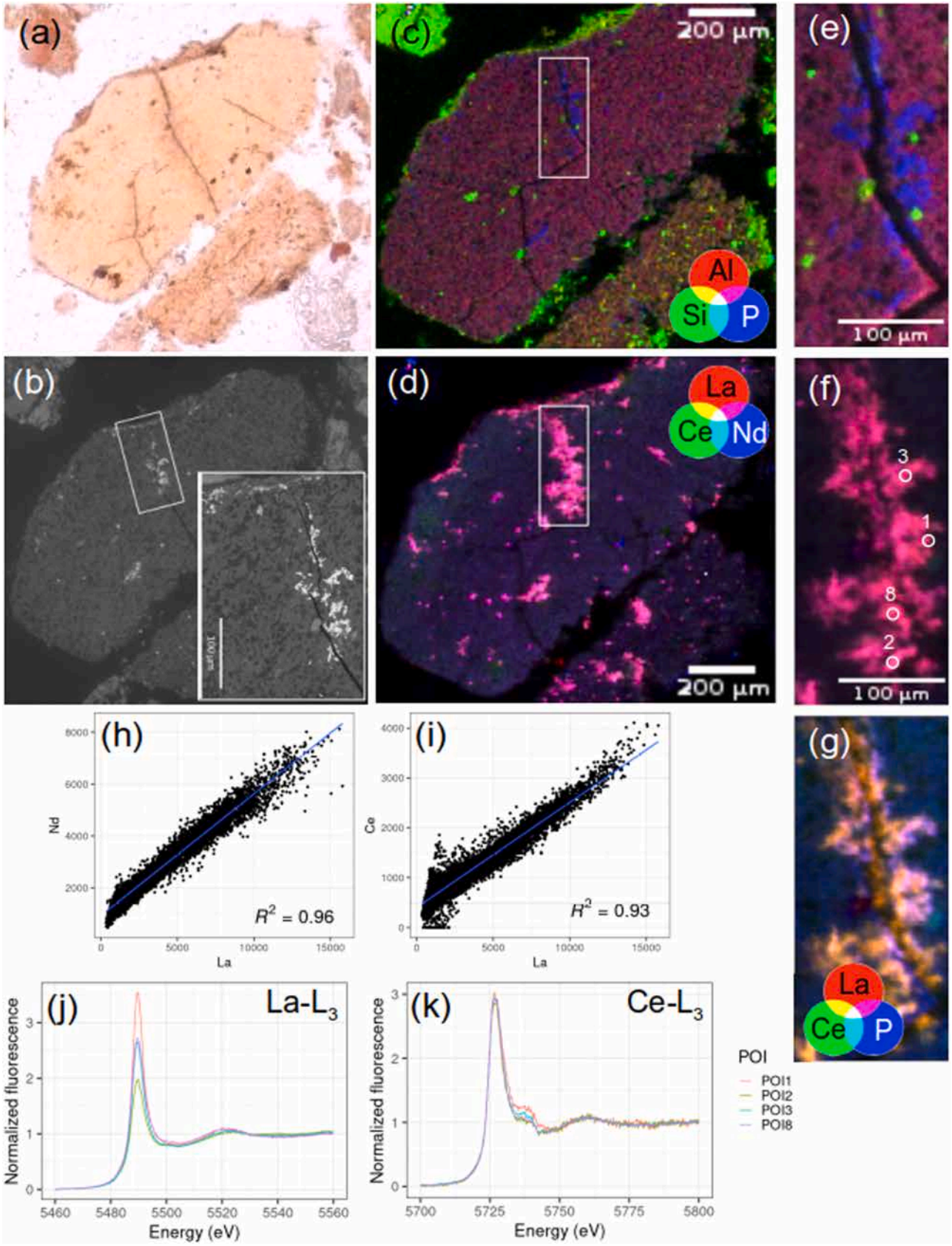

Fig. 5. Optical (a) and backscattered electronic (b) images and fluorescence maps (c-g) of an Al-rich grain containing phosphorus in the thin section made in the surface of tailings (0–6 cm) amended and planted with ramie (presented in Fig. S4–3). Corresponding elemental fluorescence maps are shown in Figures S5–5 & 6. Fluorescence signal correlation plots of La with Nd (h) and Ce (i) in the fracture region shown in f. La (j) and Ce (k) L_3-edge XANES spectra at various POIs shown in f.

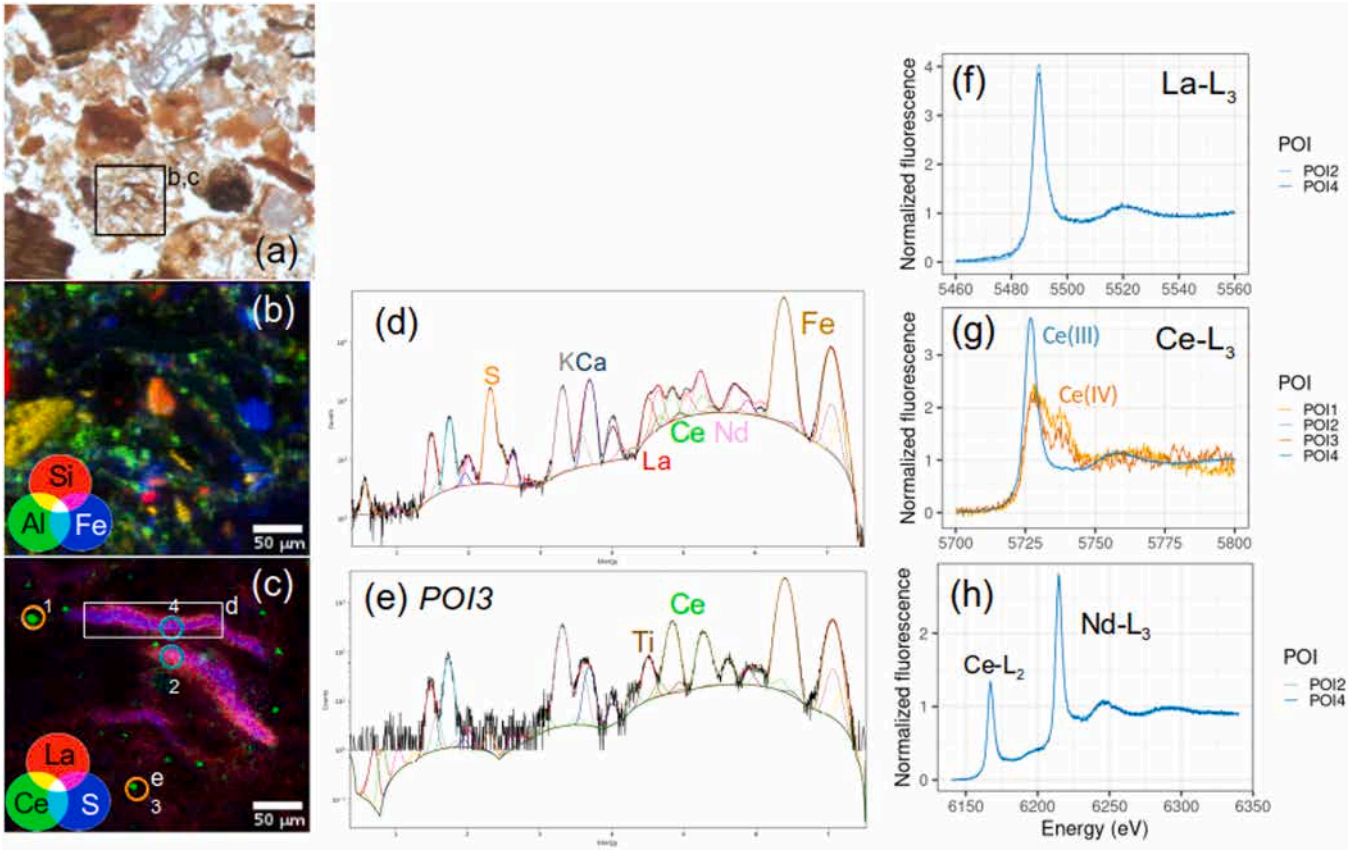

Fig. 6. Optical (a) and RGB fluorescence (b-c) maps of organic material in the thin section made in the surface of tailings (0–6 cm) amended and planted with miscanthus (presented in Fig. S4–2). Fitted whole XRF spectra of the box and POI 3 are shown in (d) and (e), respectively. La, Ce, Nd XANES spectra of several POIs are shown in (f-h).

these observations are consistent with results reported elsewhere (Zhou et al., 2023). Similar minerals (quartz, K-feldspars and phyllosilicates) were detected in weathered granite collected from an ion-adsorption ore of the same geographical area (Mukai et al., 2020).

Careful data processing of fluorescence data and whole XRF spectra peak fitting of the entire maps recorded at LUCIA beamline allowed us to detect the most abundant REEs (La, Ce, Nd), down to 50 ppm bulk concentration (for Nd) in complex media. This is, to our knowledge, the first time this type of measurements was successfully performed on undisturbed soils, directly in soil thin sections, without pre-concentration. Previous synchrotron-based analyses were carried out to study the distribution of REEs in thin sections and polished resin-mounted samples from ore material from similar deposits in Southern China and Madagascar, exhibiting bulk concentrations from 500 to 7700 mg_{REE} kg^{-1} (Borst et al., 2020; Ram et al., 2019), significantly higher than our samples, especially the Miscanthus one (Table 2). In these samples collected in similar geological context and environment, directly formed by the weathering of REE-rich granitic rock, the authors had also evidenced the heterogeneity of REE distribution, highlighting the necessity to work with undisturbed samples keeping the soil structure intact. Even by doing so, it can still be difficult to detect trivalent REEs, that are mostly diffusely dispersed throughout a fine-grained amorphous matrix around crystalline mineral phases.

Speciation of REEs in tailing samples

In this study, we focused on REE speciation in tailings issued from the lixiviation of IAD ores. Deciphering the main soil phases to which REEs are associated is crucial to develop adapted remediation or recovery strategies.

The specific behavior of Ce

Since Ce is the only element of the REEs series that can precipitate when oxidized to tetravalent Ce(IV), Ce in our samples was expected to be present mainly as cerianite (CeO_2) particles, a non-exchangeable Ce pool that could not have been leached from the ore by the ammonium sulfate solution (Li *et al.*, 2017). The positive Ce anomaly (*Ce > 1) recorded in most of the tailing samples (Table 2) confirms the relatively low migration capacity of Ce in the tailings subjected to leaching activity (Liu et al., 2019). Accordingly, macroscopic bulk analyses showed that Ce displays a different behavior, being significantly less extractable than the other REEs (Fig. 1). Initial SEM analyses showed Ce-rich particles dispersed within the soil matrix (Fig. 3), often associated with Mn and Fe. These observations were in agreement with previous studies showing that the presence of Ce(IV) in similar weathered granites is controlled by local conditions, such as rhizosphere network and associated Fe/Mn oxyhydroxides that can generate local variations of pH and oxidative conditions (Janots et al., 2015; Ram et al., 2019). Indeed, Fe and Mn (hydr)oxides can oxidize Ce(III) into Ce(IV), resulting in its precipitation as CeO_2 on their surface. For example, the co-localization of Ce and Mn in the map shown in Fig. 4 suggests that the black particle coating the quartz is a Mn oxide that may have oxidized and precipitated Ce.

In this study, we used synchrotron radiation to determine Ce speciation in the samples. Our observations evidenced two Ce pools: (i) tetravalent Ce(IV) - as CeO_2 - in well-defined micrometric grains, and (ii) trivalent Ce(III) with a more diffuse distribution and systemically co-localized with other REEs (at least La and Nd) in fine-grained matrix or organic structures. The high number of measurements performed on LUCIA beamline allows us to assert that Ce was predominantly Ce(IV) when not associated to other REEs. Assuming that both pools have different availability, extraction results suggest that Ce is mainly present

(>90 %) in non-exchangeable form (co-precipitated with Fe-Mn oxides). Thus, selective Ce recovery process from the tailings should be designed, such as Ce sulfation and Fe/Mn mineralization (Zhou et al., 2021, 2023).

Co-localization and speciation of trivalent REEs

The combination of micro-XRF (with whole XRF spectrum fitting using PyMCA) and micro-XANES was particularly powerful to evidence the association of the elements at the micrometric scale. It allowed us to certify the presence of Ce(III) together with trivalent La and Nd, even when the signal was too low to be clearly detected or readily extracted from the fit of fluorescence spectra (for example on the organic structures of Fig. 6). Indeed, by extending the energy range of Nd L_3-edge XANES spectrum to include the L_2 line of Ce, we were able to notify also the co-localisation of Ce and Nd (Figs. 4h and 6h). The absorbance edge at 6168 eV demonstrates its presence and, according to Borst et al. (2020), its oxidation state as Ce(III).

Observations on undisturbed tailing soil samples evidenced the presence of a fine-grained matrix around some mineral grains. This highly heterogeneous material is composed of submicrometric phyllosilicates (kaolinite, halloysite) and Fe (hydr)oxides that probably present a poor crystallinity, certainly leading to the presence of structure defects generating numerous surface sites to which trivalent REEs species can bind. These phases may present specific and reactive adsorption sites that prevent REE leaching by the acidic treatment solution. Our observations concur with the ones from Borst et al. (2020), who analysed Y K-edge XANES spectra of leached samples and concluded that the non-leachable REEs in the soils are probably strongly bound as inner-sphere complexes onto surfaces of kaolinite, halloysite or Fe-Mn oxyhydroxides.

The association of REEs with phosphates was not unexpected in our samples, since phosphates are common bearing phases for REEs and accessory minerals in the parent granite (Ishihara et al., 2008; Li et al., 2017). However, it cannot be excluded that the phosphates found in the tailings could have been formed by secondary precipitation of acidic dissolved phosphates, or brought to the soil by the amendment during the remediation practices. Overall, in those tailings, REEs are not exchangeable (Fig. 1), but more probably covalently-bound to mineral phases (phyllosilicates, Fe-Mn oxyhydroxides, phosphates) and, as such, not recovered by the mining leaching process.

Impacts of reclamation practices on REE fate

The reclamation practices tested on this demonstration site – addition of organic amendment and planting of native or economic plants – had a significant effect on soil biogeochemistry and physico-chemical parameters such as an increase in C, nutrient content and pH, and a decrease in exchangeable Al concentration (Table 1). These changes, which are beneficial for plant development, are more marked in the tailings planted with ramie, which were amended twice with higher rate of amendment than those planted with miscanthus. Plant and root growth can also have an impact on the physical stability of tailings (phytostabilization), limiting erosion processes and thus environmental dispersion of REEs (Liu et al., 2022).

The reclamation practices indeed impact REE behavior at the macroscopic scale, as evidenced by the decrease of the $CaCl_2$-extractible proportion of REEs in samples that have received amendment (Fig. 1), thus implying a lower availability and associated risk of environmental dispersion of REEs in reclaimed samples. Several hypotheses can explain this observation, that are not exclusive: pH increase induced by amendment, or addition of negatively charged organic phases with high affinity for positively charged REEs (Madejón et al., 2009; Liu et al., 2022). Amendments are also a source of phosphates that can complex REEs in soils (Edahbi et al., 2018). The millimolar $CaCl_2$ extraction concentration used here led to relatively low amounts of REEs that can be readily released to the soil solution compared to the total concentration of residual REEs in the samples. However, it has been shown on tailings of the same site that >40 % of the REEs can be mobilized by ion-exchange using more concentrated saline solutions, such as 1 M $MgCl_2$ (Liu et al., 2019) or 0.5 M $(NH_4)_2SO_4$ (Zhou et al., 2023), with the exception of less available Ce, oxidized and associated with Fe and Mn oxides.

Micro-XRF measurements confirmed the enrichment in REEs on some organic residues or plant debris (Fig. 6, Figures S5–3 and S5–9). This was expected due to the known high affinity of REEs for natural organic matter (Catrouillet et al., 2020; Lin et al., 2022; Tadayon et al., 2024). Our observations are consistent with the analysis of roots of plants grown in the amended tailings at the same site, which showed accumulation of REEs by roots of *Boehmeria nivea* L. (ramie) (Liu et al., 2022) and *Miscanthus sinensis* (unpublished data). They are also in agreement with observations made in nearby province of Guangdong showing a correlation between REE enrichment in various soils and their organic matter content (Lin et al., 2022). The transfer of REEs from soil to plant has also been evidenced in similar environments, illustrating the risk of REE contamination of the food chain in case of edible plants (Wang et al., 2022).

Overall, reclamation through soil organic amendment decreases REEs availability in the topsoil, and their leaching risk in the environment. The presence of a perennial vegetation cover increases the stability of the tailings and limits erosion. However, accumulation of REEs in plant aerial parts may generate an additional REE input into soil *via* litter degradation that needs to be considered. It is thus be critical to perform a long-term survey of REEs behavior in reclaimed tailings to evaluate the sustainability of reclamation practices.

Conclusion

Mining of REE ion-adsorption deposits in South China has resulted in large amounts of tailings for which the speciation and bioavailability of residual REEs are unknown, while this information is crucial for designing sustainable reclamation. In this study, we analyzed samples from unreclaimed and reclaimed tailings (with organic amendment and vegetation planting) from a demonstration site in the Dingnan County of Ganzhou city, Jiangxi province. Using synchrotron-based micro-spectroscopy, our results showed the localization and chemical speciation of La, Ce and Nd in undisturbed soil thin sections, evidencing two pools of Ce, Ce(III) and Ce(IV). Hotspots of Ce(IV) were detected as individual grains dispersed within the soil, occasionally co-localized with Fe/Mn (hydr)oxides phases. Trivalent Ce(III) was found associated with other REEs (La, Nd) and dispersed within a fine-grained matrix, embedding larger primary minerals, and attributed to weathering by-products. Moreover, the impact of reclamation practices was clearly characterized, since, in amended and planted tailing samples, REEs were associated with organic debris and plant structures. Overall, we show here that micro-spectroscopy is a complementary tool to micro-fluorescence mapping for unravelling REE presence and co-localization, as well as their speciation. By combining in-situ measurements on thin sections and synchrotron-based spectroscopy, we managed to decipher micron-scale localization and speciation of REEs, allowing to evidence their association with mineral assemblages and organic matter. These results highlight the impact of reclamation, especially phytoremediation, and will help to design sustainable practices. Further work is now needed to determine the fate and availability of these REEs in reclaimed tailings over the longer term.

CRediT authorship contribution statement

Noémie Janot: Writing – review & editing, Writing – original draft, Visualization, Methodology, Investigation, Funding acquisition, Conceptualization. **Hermine Huot:** Writing – review & editing, Writing – original draft, Visualization, Methodology, Investigation, Conceptualization. **Camille Rivard:** Writing – review & editing, Visualization, Validation, Methodology. **Mathilde Perrin:** Investigation. **Alexandra**

Noirault: Writing – review & editing, Investigation. **Ye-Tao Tang:** Writing – review & editing, Funding acquisition, Conceptualization. **Françoise Watteau:** Writing – review & editing, Writing – original draft, Visualization, Methodology, Investigation, Funding acquisition, Conceptualization. **Emmanuelle Montargès-Pelletier:** Writing – review & editing, Writing – original draft, Visualization, Methodology, Investigation, Funding acquisition, Conceptualization.

Declaration of competing interest

The authors declare that they have no known competing financial interests or personal relationships that could have appeared to influence the work reported in this paper.

Acknowledgments

We acknowledge the financial support from the French National Research Agency through the national program "Investissements d'avenir" with the reference ANR-10-LABX-21–01/LABEX RESSOURCES21. This work is supported by the Fundamental Research Funds for Colleges and Universities, Young Teacher Training Program of Sun Yat-sen University [Grant No. 171gpy90]; International Young Scientists Fund of the National Natural Science Foundation of China [Grant No. 21850410450]; the National Key Research and Development Program of China of Jiangxi province [Grant No. 20192ACB70016], the National Natural Science Foundation of China (NSFC) [Grant No. 41771343] and Guangdong Province Science and Technology Program [Grant No. 2022A0505090002]. The "International Joint Lab-ECOLAND" is acknowledged for supporting this work.

We acknowledge the work of our colleagues Adeline Bouchard, Romain Goudon, Lucas Charrois, Jean-Claude Begin (LSE, Vandœuvre) and Renaud Gley (LIEC, Vandœuvre) for sample preparation and analyses. We also acknowledge Sylvie Migot (Institut Jean Lamour, Nancy) for TEM investigations.

We acknowledge SOLEIL synchrotron (proposal 20191995) and Stanford Synchrotron Radiation Lightsource (SSRL, proposal 5299A) for provision of synchrotron radiation facilities and we would like to thank Sharon Bone for assistance in using beamline 2–3 at SSRL for preliminary work.

Funding sources

French National Research Agency through the national program "Investissements d'avenir" with the reference ANR-10-LABX-21–01/LABEX RESSOURCES21; Fundamental Research Funds for Colleges and Universities, Young Teacher Training Program of Sun Yat-sen University [Grant No. 171gpy90]; International Young Scientists Fund of the National Natural Science Foundation of China [Grant No. 21850410450]; National Key Research and Development Program of China of Jiangxi province [Grant No. 20192ACB70016]; National Natural Science Foundation of China (NSFC) [Grant No. 41771343]; Guangdong Province Science and Technology Program [Grant No.2022A0505090002].

Supplementary materials

Supplementary material associated with this article can be found, in the online version, at doi:10.1016/j.hazadv.2025.100609.

Data availability

Data will be made available on request.

References

Berger, A., Janots, E., Gnos, E., Frei, R., Bernier, F., 2014. Rare earth element mineralogy and geochemistry in a laterite profile from Madagascar. Appl. Geochem. 41, 218–228. https://doi.org/10.1016/j.apgeochem.2013.12.013.

Borst, A.M., Smith, M.P., Finch, A.A., Estrade, G., Villanova-de-Benavent, C., Nason, P., Marquis, E., Horsburgh, N.J., Goodenough, K.M., Xu, C., Kynický, J., Geraki, K., 2020. Adsorption of rare earth elements in regolith-hosted clay deposits. Nat. Commun. 11, 4386. https://doi.org/10.1038/s41467-020-17801-5.

Bullock, P., Fedoroff, N., Jongerius, A., 1985. Handbook for Soil Thin Section Description. Waine.

Catrouillet, C., Guenet, H., Pierson-Wickmann, A.-C., Dia, A., LeCoz, M.B., Deville, S., Lenne, Q., Suko, Y., Davranche, M., Catrouillet, C., Guenet, H., Pierson-Wickmann, A.-C., Dia, A., LeCoz, M.B., Deville, S., Lenne, Q., Suko, Y., Davranche, M., 2020. Rare earth elements as tracers of active colloidal organic matter composition. Environ. Chem. 17, 133–139. https://doi.org/10.1071/EN19159.

Chi, R., Tian, J., Li, Z., Peng, C., Wu, Y., Li, S., Wang, C., Zhou, Z., 2005. Existing State and partitioning of rare earth on weathered ores. J. Rare Earths 23, 756–760.

Edahbi, M., Plante, B., Benzaazoua, M., Ward, M., Pelletier, M., 2018. Mobility of rare earth elements in mine drainage: influence of iron oxides, carbonates, and phosphates. Chemosphere 199, 647–654. https://doi.org/10.1016/j.chemosphere.2018.02.054.

Galhardi, J.A., Leles, B.P., de Mello, J.W.V., Wilkinson, K.J., 2020. Bioavailability of trace metals and rare earth elements (REE) from the tropical soils of a coal mining area. Sci. Total Environ. 717, 134484. https://doi.org/10.1016/j.scitotenv.2019.134484.

Giraudoux, P., 2023. pgirmess: spatial analysis and data mining for field ecologists.

Gómez-Ariza, J.L., Giráldez, I., Sánchez-Rodas, D., Morales, E., 1999. Metal readsorption and redistribution during the analytical fractionation of trace elements in oxic estuarine sediments. Anal. Chim. Acta 399, 295–307. https://doi.org/10.1016/S0003-2670(99)00460-2.

Guo, M., 2022. Aggregation and Biological Processes in Ion- Adsorption Rare Earth Mine Tailings Under Natural Restoration and Reclamation Approaches (PhD Thesis). Université de Lorraine. https://www.theses.fr/2022LORR0301.

Guo, M.-N., Zhong, X., Liu, W.-S., Wang, G.-B., Chao, Y.-Q., Huot, H., Qiu, R.-L., Morel, J. L., Watteau, F., Séré, G., Tang, Y.-T., 2022. Biogeochemical dynamics of nutrients and rare earth elements (REEs) during natural succession from biocrusts to pioneer plants in REE mine tailings in southern China. Sci. Total. Environ. 828, 154361. https://doi.org/10.1016/j.scitotenv.2022.154361.

Huang, J., He, H., Tan, W., Liang, X., Ma, L., Wang, Y., Qin, X., Zhu, J., 2021. Groundwater controls REE mineralisation in the regolith of South China. Chem. Geol. 577, 120295. https://doi.org/10.1016/j.chemgeo.2021.120295.

Ishihara, S., Hua, R., Hoshino, M., Murakami, H., 2008. REE abundance and REE minerals in granitic rocks in the Nanling Range, Jiangxi Province, Southern China, and generation of the REE-rich weathered crust deposits. Resource Geol. 58, 355–372. https://doi.org/10.1111/j.1751-3928.2008.00070.x.

Jally, B., Laubie, B., Chour, Z., Muhr, L., Qiu, R., Morel, J.L., Tang, Y., Simonnot, M.-O., 2021. A new method for recovering rare earth elements from the hyperaccumulating fern dicranopteris linearis from China. Miner. Eng. 166, 106879. https://doi.org/10.1016/j.mineng.2021.106879.

Janots, E., Bernier, F., Brunet, F., Muñoz, M., Trcera, N., Berger, A., Lanson, M., 2015. Ce (III) and Ce(IV) (re)distribution and fractionation in a laterite profile from Madagascar: insights from *in situ* XANES spectroscopy at the Ce LIII-edge. Geochim. Cosmochim. Acta 153, 134–148. https://doi.org/10.1016/j.gca.2015.01.009.

Jowitt, S.M., Wong, V.N.L., Wilson, S.A., Gore, O., 2017. Critical metals in the critical zone: controls, resources and future prospectivity of regolith-hosted rare earth elements. Austral. J. Earth Sci. 64, 1045–1054. https://doi.org/10.1080/08120099.2017.1380701.

Kanazawa, Y., Kamitani, M., 2006. Rare earth minerals and resources in the world. J. Alloys Compd. 1339–1343. https://doi.org/10.1016/j.jallcom.2005.04.033, 408–412.

Lachaux, N., Catrouillet, C., Marsac, R., Poirier, L., Pain-Devin, S., Gross, E.M., Giamberini, L., 2022a. Implications of speciation on rare earth element toxicity: a focus on organic matter influence in Daphnia magna standard test. Environ. Pollut. 307, 119554. https://doi.org/10.1016/j.envpol.2022.119554.

Lachaux, N., Cossu-Leguille, C., Poirier, L., Gross, E.M., Giamberini, L., 2022b. Integrated environmental risk assessment of rare earth elements mixture on aquatic ecosystems. Front. Environ. Sci. 10. https://doi.org/10.3389/fenvs.2022.974191.

Lachaux, N., Otero-Fariña, A., Minguez, L., Sohm, B., Rétif, J., Châtel, A., Poirier, L., Devin, S., Pain-Devin, S., Gross, E.M., Giamberini, L., 2023. Fate, subcellular distribution and biological effects of rare earth elements in a freshwater bivalve under complex exposure. Sci. Total Environ. 905, 167302. https://doi.org/10.1016/j.scitotenv.2023.167302.

Laveuf, C., Cornu, S., 2009. A review on the potentiality of Rare Earth Elements to trace pedogenetic processes. Geoderma 154, 1–12. https://doi.org/10.1016/j.geoderma.2009.10.002.

Li, M.Y.H., Zhou, M.-F., 2020. The role of clay minerals in formation of the regolith-hosted heavy rare earth element deposits. Am. Mineralogist 105, 92–108. https://doi.org/10.2138/am-2020-7061.

Li, M.Y.H., Zhou, M.-F., Williams-Jones, A.E., 2020. Controls on the dynamics of rare earth elements during subtropical hillslope processes and formation of regolith-hosted deposits. Econ. Geol. 115, 1097–1118. https://doi.org/10.5382/econgeo.4727.

Li, Y.H.M., Zhao, W.W., Zhou, M.-F., 2017. Nature of parent rocks, mineralization styles and ore genesis of regolith-hosted REE deposits in South China: an integrated genetic

model. J. Asian Earth. Sci. 148, 65–95. https://doi.org/10.1016/j.jseaes.2017.08.004.
Lin, Z., Wei, G., Zhang, J., Liang, X., Huang, G., 2022. Origin and distribution of rare earth elements (REEs) in the soils of Meizhou City, southern China with high abundance of regolith-hosted REEs. Appl. Geochem. 147, 105514. https://doi.org/10.1016/j.apgeochem.2022.105514.
Liu, C., Liu, W.-S., Huot, H., Guo, M.-N., Zhu, S.-C., Zheng, H.-X., Morel, J.L., Tang, Y.-T., Qiu, R.-L., 2022. Biogeochemical cycles of nutrients, rare earth elements (REEs) and Al in soil-plant system in ion-adsorption REE mine tailings remediated with amendment and ramie (Boehmeria nivea L.). Sci. Total Environ. 809, 152075. https://doi.org/10.1016/j.scitotenv.2021.152075.
Liu, C., Yuan, M., Liu, W.-S., Guo, M.-N., Huot, H., Tang, Y.-T., Laubie, B., Simonnot, M.-O., Morel, J.L., Qiu, R.-L., 2018. Element case studies: rare earth elements. In: Van der Ent, A., Echevarria, G., Baker, A.J.M., Morel, J.L. (Eds.), Agromining: Farming for Metals. Springer International Publishing, Cham, pp. 297–308. https://doi.org/10.1007/978-3-319-61899-9_19.
Liu, W.-S., Guo, M.-N., Liu, C., Yuan, M., Chen, X.-T., Huot, H., Zhao, C.-M., Tang, Y.-T., Morel, J.L., Qiu, R.-L., 2019. Water, sediment and agricultural soil contamination from an ion-adsorption rare earth mining area. Chemosphere 216, 75–83. https://doi.org/10.1016/j.chemosphere.2018.10.109.
Liu, W.-S., Chen, Y.-Y., Huot, H., Liu, C., Guo, M.-N., Qiu, R.-L., Morel, J.L., Tang, Y.-T., 2020a. Phytoextraction of rare earth elements from ion-adsorption mine tailings by Phytolacca americana: effects of organic material and biochar amendment. J. Clean. Prod. 275, 122959. https://doi.org/10.1016/j.jclepro.2020.122959.
Liu, Y., Zhong, X., Huot, H., Liu, W., Liu, C., Guo, M., Li, Y., Fei, Y., Chao, Y., Wang, S., Tang, Y., Qiu, R., 2020b. Reclamation with organic amendments and plants remodels the diversity and structure of bacterial community in ion-adsorption rare earth element mine tailings. J. Soils. Sediments. 20, 3669–3680. https://doi.org/10.1007/s11368-020-02704-1.
Madejón, E., Madejón, P., Burgos, P., Pérez de Mora, A., Cabrera, F., 2009. Trace elements, pH and organic matter evolution in contaminated soils under assisted natural remediation: a 4-year field study. J. Hazard. Mater. 162, 931–938. https://doi.org/10.1016/j.jhazmat.2008.05.119.
Moldoveanu, G.A., Papangelakis, V.G., 2013. Recovery of rare earth elements adsorbed on clay minerals: II. Leaching with ammonium sulfate. Hydrometallurgy 158–166. https://doi.org/10.1016/j.hydromet.2012.10.011, 131–132.
Mukai, H., Kon, Y., Sanematsu, K., Takahashi, Y., Ito, M., 2020. Microscopic analyses of weathered granite in ion-adsorption rare earth deposit of Jianxi Province, China. Sci. Rep. 10, 20194. https://doi.org/10.1038/s41598-020-76981-8.
Murakami, H., Ishihara, S., 2008. REE mineralization of weathered crust and clay sediment on granitic rocks in the Sanyo Belt, SW Japan and the Southern Jiangxi Province, China. Resource Geol. 58, 373–401. https://doi.org/10.1111/j.1751-3928.2008.00071.x.
Nie, W., Zhang, R., He, Z., Zhou, J., Wu, M., Xu, Z., Chi, R., Yang, H., 2020. Research progress on leaching technology and theory of weathered crust elution-deposited rare earth ore. Hydrometallurgy 193, 105295. https://doi.org/10.1016/j.hydromet.2020.105295.
Ou, X., Chen, Zhibiao, Chen, X., Li, X., Wang, J., Ren, T., Chen, H., Feng, L., Wang, Y., Chen, Zhiqiang, Liang, M., Gao, P., 2022. Redistribution and chemical speciation of rare earth elements in an ion–adsorption rare earth tailing, Southern China. Sci. Total Environ. 821, 153369. https://doi.org/10.1016/j.scitotenv.2022.153369.
Pan, J., Zhao, L., Li, Z., Huang, X., Feng, Z., Chen, J., 2023. Occurrence and vertical distribution of aluminum and rare earths in weathered crust elution-deposited rare earth ore: effect of soil solution pH and clay minerals. J. Rare Earth. https://doi.org/10.1016/j.jre.2023.06.016.
R Core Team, 2022. R: a language and environment for statistical computing.
Ram, R., Becker, M., Brugger, J., Etschmann, B., Burcher-Jones, C., Howard, D., Kooyman, P.J., Petersen, J., 2019. Characterisation of a rare earth element- and zirconium-bearing ion-adsorption clay deposit in Madagascar. Chem. Geol. 522, 93–107. https://doi.org/10.1016/j.chemgeo.2019.05.011.
Ravel, B., Newville, M., 2005. ATHENA, ARTEMIS, HEPHAESTUS: data analysis for X-ray absorption spectroscopy using IFEFFIT. J. Synchrotron. Radiat. 537–541. https://doi.org/10.1107/S0909049505012719.
Riesgo García, M.V., Krzemień, A., Manzanedo del Campo, M.Á., Menéndez Álvarez, M., Gent, M.R., 2017. Rare earth elements mining investment: it is not all about China. Resour. Policy. 53, 66–76. https://doi.org/10.1016/j.resourpol.2017.05.004.
Sanematsu, K., Kon, Y., Imai, A., Watanabe, K., Watanabe, Y., 2013. Geochemical and mineralogical characteristics of ion-adsorption type REE mineralization in Phuket, Thailand. Miner. Deposita 48, 437–451. https://doi.org/10.1007/s00126-011-0380-5.
Sanematsu, K., Murakami, H., Watanabe, Y., Duangsurigna, S., Siphandone, V., 2009. Enrichment of rare earth elements (REE) in granitic rocks and their weathered crusts in central and southern Laos. Bull. Geol. Surv. Japan 60, 527–558. https://doi.org/10.9795/bullgsj.60.527.
Sanematsu, K., Watanabe, Y., 2016. Characteristics and genesis of ion adsorption-type rare earth element deposits. In: Verplanck, P.L., Hitzman, M.W. (Eds.), Rare Earth and Critical Elements in Ore Deposits. Society of Economic Geologists, p. 0. https://doi.org/10.5382/Rev.18.03.
Schindelin, J., Arganda-Carreras, I., Frise, E., Kaynig, V., Longair, M., Pietzsch, T., Preibisch, S., Rueden, C., Saalfeld, S., Schmid, B., Tinevez, J.-Y., White, D.J., Hartenstein, V., Eliceiri, K., Tomancak, P., Cardona, A., 2012. Fiji: an open-source platform for biological-image analysis. Nat. Methods 9, 676–682. https://doi.org/10.1038/nmeth.2019.
Segovia, C., Hedri, M., Huot, H., Zigler-Devin, I., Liu, C., Tang, Y., Qiu, R., Morel, J.L., Brosse, N., 2021. Industrial ramie growing on reclaimed ion-adsorption rare earth elements mine tailings in southern china: defibration and fibers quality. Waste Biomass Valor. https://doi.org/10.1007/s12649-021-01442-w.
Solé, V.A., Papillon, E., Cotte, M., Walter, Ph., Susini, J., 2007. A multiplatform code for the analysis of energy-dispersive X-ray fluorescence spectra. Spectrochimica Acta Part B: Atomic Spectrosc. 62, 63–68. https://doi.org/10.1016/j.sab.2006.12.002.
Stoops, G., Marcelino, V., Mees, F., 2010. ScienceDirect (Online service) (Eds.). Interpretation of Micromorphological Features of Soils and Regoliths. Elsevier, Amsterdam ; Oxford.
Stuckman, M.Y., Lopano, C.L., Granite, E.J., 2018. Distribution and speciation of rare earth elements in coal combustion by-products via synchrotron microscopy and spectroscopy. Int. J. Coal. Geol. 195, 125–138. https://doi.org/10.1016/j.coal.2018.06.001.
Tadayon, Y., Vantelon, D., Gigault, J., Dia, A., Pattier, M., Dutruch, L., Davranche, M., 2024. Rare earth elements interaction with iron-organic matter colloids as a control of the REE environmental dissemination. J. Colloid Interface Sci. 655, 70–79. https://doi.org/10.1016/j.jcis.2023.10.110.
Taylor, S.R., McLennan, S.M., 1995. The geochemical evolution of the continental crust. Rev. Geophys. 33, 241–265. https://doi.org/10.1029/95RG00262.
Voßenkaul, D., Stoltz, N., Meyer, F., Friedrich, B., 2015. Extraction of rare earth elements from non- Chinese ion adsorption clays. In: Presented at the European Metallurgical Conference, Düsseldorf. https://doi.org/10.13140/RG.2.1.1177.6401.
Wang, D., Zhao, Z., Yu, Y., Dai, J., Deng, M., Zhao, T., Liu, L., 2018. Exploration and research progress on ion-adsorption type REE deposit in South China. China Geol. 1, 414–423. https://doi.org/10.31035/cg2018022.
Wang, Y., Wang, G., Sun, M., Liang, X., He, H., Zhu, J., Takahashi, Y., 2022. Environmental risk assessment of the potential “Chemical time bomb” of ion-adsorption type rare earth elements in urban areas. Sci. Total Environ. 822, 153305. https://doi.org/10.1016/j.scitotenv.2022.153305.
Wei, F.S., Liu, T.L., Teng, E.J., Rui, K.S., 1991. 15 rare earth elements in Chinese soil. Environ. Sci. 12, 78–82. https://doi.org/10.13227/j.hjkx.1991.05.024 (in Chinese).
Wu, Z., Chen, Y., Wang, Y., Xu, Y., Lin, Z., Liang, X., Cheng, H., 2023. Review of rare earth element (REE) adsorption on and desorption from clay minerals: application to formation and mining of ion-adsorption REE deposits. Ore Geol. Rev. 157, 105446. https://doi.org/10.1016/j.oregeorev.2023.105446.
Yang, X.J., Lin, A., Li, X.-L., Wu, Y., Zhou, W., Chen, Z., 2013. China’s ion-adsorption rare earth resources, mining consequences and preservation. Environ. Dev. 8, 131–136. https://doi.org/10.1016/j.envdev.2013.03.006.
Zhou, L., Li, Z., Liu, W., Liu, S., Zhang, L., Zhong, L., Luo, X., Liang, H., 2015. Restoration of rare earth mine areas: organic amendments and phytoremediation. Environ. Sci. Pollut. Res. 22, 17151–17160. https://doi.org/10.1007/s11356-015-4875-y.
Zhou, F., Xiao, Y., Guo, M., Tang, Y., Zhang, W., Qiu, R., 2021. Selective leaching of rare Earth elements from ion-adsorption rare earth tailings: a synergy between CeO_2 reduction and Fe/Mn stabilization. Environ. Sci. Technol. 55, 11328–11337. https://doi.org/10.1021/acs.est.1c03106.
Zhou, F., Xiao, Y., Guo, M., Wang, S., Qiu, R., Morel, J.-L., Simonnot, M.-O., Zhang, W.-X., Zhang, W., Tang, Y.-T., 2023. Insights into the selective transformation of ceria sulfation and iron/manganese mineralization for enhancing the selective recovery of rare earth elements. Environ. Sci. Technol. 57, 3357–3368. https://doi.org/10.1021/acs.est.2c08395.